Science of the Total Environment 754 (2021) 142411

Contents lists available at ScienceDirect

Science of the Total Environment

journal homepage: www.elsevier.com/locate/scitotenv

Climatic, land cover, and anthropogenic controls on dissolved organic matter quantity and quality from major alpine rivers across the Himalayan-Tibetan Plateau

Meilian Chen [a,*], Chaoliu Li [b,c], Robert G.M. Spencer [d], Nagamitsu Maie [e], Jin Hur [f], Amy M. McKenna [g], Fangping Yan [h]

[a] Environmental Program, Guangdong Technion - Israel Institute of Technology, Shantou 515063, China
[b] CAS Key Laboratory of Tibetan Environment Changes and Land Surface Processes, Institute of Tibetan Plateau Research, Chinese Academy of Sciences, Beijing 100101, China
[c] CAS Center for Excellence in Tibetan Plateau Earth Sciences, Chinese Academy of Sciences, Beijing 100101, China
[d] Department of Earth, Ocean and Atmospheric Science, Florida State University, Tallahassee, FL 32306, United States
[e] School of Veterinary Medicine, Kitasato University, 23-35-1 Higashi, Towada, Aomori 034-8628, Japan
[f] Department of Environment & Energy, Sejong University, Seoul 05006, South Korea
[g] National High Magnetic Field Laboratory, Tallahassee, Florida 32310, United States
[h] State Key Laboratory of Cryospheric Sciences, Northwest Institute of Eco-Environment and Resources, Chinese Academy of Sciences, Lanzhou 730000, China

HIGHLIGHTS

- We revealed a general increasing trend of DOC juxtaposed to a decreasing trend of aromaticity with latitude.
- Proglacial tributaries were found to be relatively dominated by tyrosine-like FDOM.
- Rivers within larger catchment basins were more controlled by humic-like FDOM.
- High condensed aromatics indicated black soot pollution of alpine rivers.
- DOM are controlled by climate, land cover, and anthropogenic activities.

GRAPHICAL ABSTRACT

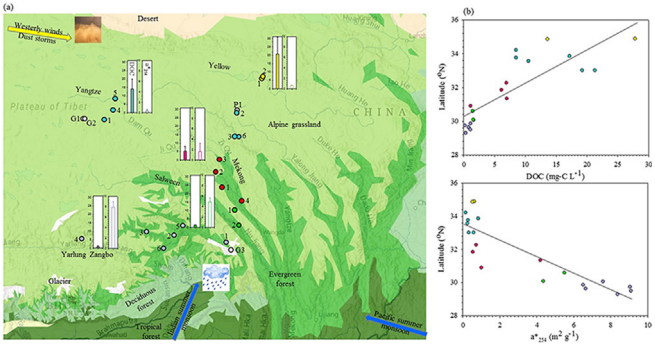

ARTICLE INFO

Article history:
Received 5 August 2020
Received in revised form 15 September 2020
Accepted 16 September 2020
Available online 18 September 2020

Editor: Fernando A.L. Pacheco

Keywords:
DOM
Glacier
Permafrost
EEM-PARAFAC
FT-ICR MS
Dust storm

ABSTRACT

Alpine rivers in mountainous regions are crucial not only for land-ocean transfer of chemical species and sediments, but also for water, food, and energy security. Here, we examined dissolved organic matter (DOM) from the major alpine waters on the Tibetan Plateau. Our results revealed a decreasing trend of DOM quantity juxtaposed to an increasing trend of aromaticity from the northern to southern plateau. This is potentially caused by a general decreasing gradient of dust load combined with an increasing gradient of precipitation and vegetation from the NW to SE plateau. Furthermore, most proglacial streams and smaller tributaries were found to be relatively dominated by tyrosine-like fluorescent DOM from glaciers. In contrast, most main stems of rivers and tributaries within larger catchment basins were more controlled by humic-like fluorescent DOM from terrestrial origins. Condensed aromatics accounts for 14–21% of molecular formulas for riverine DOM, much higher than the world's average of ~11%, which indicated anthropogenic black soot pollution. In addition, there is a higher level of DOM amount in the monsoon season than in winter, and DOM characteristics varied more widely (dissolved organic carbon concentration: 0.2-37 mg-C L^{-1}, Fluorescence Index: 1.2-1.8) on the Tibetan Plateau in comparison to other global alpine watersheds. This suggests heterogeneous land cover, anthropogenic, and climatic factors at play, which is reflected in DOM quantity and quality, over the highest plateau on Earth.

* Corresponding author.
E-mail address: chen.meilian@gtiit.edu.cn (M. Chen).

https://doi.org/10.1016/j.scitotenv.2020.142411
0048-9697/

Nomenclature

A. Acronym in alphabetic order

CDOM	chromophoric dissolved organic matter
DOC	dissolved organic carbon
DOM	dissolved organic matter
EC	electrical conductivity
EEM-PARAFAC	excitation emission matrix-parallel factor analysis
FDOM	fluorescent dissolved organic matter
FT-ICR MS	Fourier transform ion cyclotron resonance mass spectrometry
HTP	Himalayan-Tibetan Plateau
MR	Mekong River
SR	Salween River
UV–Vis	ultraviolet-visible spectroscopy
YR	Yellow River (Huang River)
YT	Yangtze River (Chang River)
YZ	Yarlung Zangbo River (upstream of Brahmaputra River)

B. DOM compound categories

Aliphatics	$O/C < 0.9$, $H/C > 1.5$, $N = 0$
Peptides	$O/C < 0.9$, $H/C > 1.5$, $N > 0$
Highly unsaturated	$AI_m < 0.5$, $H/C \leq 1.5$
Polyphenols	$0.67 > AI_m > 0.5$
Condensed aromatics	$AI_m \geq 0.67$

C. DOM indices

DBE	double bond equivalent; $DBE = 1 + 0.5(2C - H + N)$
AI_m	modified aromatic index; $AI_m = (1 + C - 0.5O - S - 0.5H)/(C - 0.5O - S - N - P)$
FI	fluorescence index. A proxy for fulvic acids sources; $FI = F_{450}/F_{500}$ at excitation 370 nm, F_λ represents emission intensity at wavelength of λ nm
BIX	biological index. A proxy for recent biological activities; $BIX = F_{380}/F_{430}$ at excitation 310 nm
HIX	humification index. A proxy for degree of humification; $HIX = \Sigma F_{435-480}/\Sigma F_{300-345}$ at excitation 255 nm
S_R	slope ratio. A proxy for molecular weight of CDOM; slope ratio of absorbance (275–295 nm to 350–400 nm)
a_λ	absorption coefficient at wavelength λ nm; a_λ = 2.303 × absorbance at 254 nm
a^*_{254}	specific absorption coefficient at wavelength 254 nm; $a^*_{254} = a_{254}$ normalized to DOC concentration

1. Introduction

Mountain regions, serving as water towers for the world, are highly vulnerable to climate change (Messerli et al., 2004). Alpine rivers flowing at altitude and through mountainous landscapes are at a crossroads facing many issues and challenges with retreating glaciers, thawing permafrost, increased human activities, and other cascading ecosystem and climatic responses triggered by natural and anthropogenic stressors (Qiu, 2008; Immerzeel et al., 2010; Mukherji et al., 2015; Su et al., 2016; Chen et al., 2019). It has been shown that from glaciated environments the annual release of dissolved organic carbon (DOC) is dominated by mountain glaciers with an estimated 15 Tg of DOC loss by 2050 (Hood et al., 2015). Furthermore, the permafrost zone delivers ~100 Tg C yr^{-1} permafrost-derived DOC to fluvial systems with ~36 Tg C yr^{-1} reaching the ocean (Holmes et al., 2012; Abbott et al., 2016). As rivers are cradles of civilization and alpine rivers are crucial for water, food, and energy security both upstream and downstream, it is critical to study them for water quality and sustainable environmental development.

Dissolved organic matter (DOM) in alpine rivers is mainly derived from glacier runoff, permafrost thaw, vegetation and soil leaching, and atmospheric wet and dry deposition. Terrestrial-derived DOM from soils and vegetation can enter the fluvial systems via not only hydrological flow paths during rainfall and glacier melt, but also aeolian dust deposition. It has been reported that glacier-derived DOM may be ancient yet biolabile with up to ~70% bioavailable DOC (BDOC, Hood et al., 2009; Spencer et al., 2014), derived from microbial products and inputs from anthropogenic aerosols (Lafrenière and Sharp, 2004; Stubbins et al., 2012; Feng et al., 2016). Furthermore, the high bioavailability of glacier-derived DOM may prime degradation of terrestrial-derived DOM (Bianchi, 2011; Hood et al., 2015). In comparison, permafrost-derived DOC exhibits ~22% BDOC, with BDOC from deeper permafrost generally higher than that from active layer (Liu et al., 2019).

The Himalayan-Tibetan Plateau (HTP), with an area of ~2.5×10^6 km^2, hosts the most extensive mountainous areas in the world. It is the origin of numerous streams and rivers including major world rivers such as the Yangtze River, Yellow River, Mekong River, and Brahmaputra River. It plays a crucial role in water resource (for >1.4 billion residents), climate, and carbon budget at a regional and even global scale (Thompson et al., 2000; Kang et al., 2010). There are ~36,800 mountain glaciers in the HTP, with an area of 49,873 km^2 and a volume of 4560 km^3 (Yao et al., 2007). Due to the warming at ~0.30-0.45 °C per decade over the past 50 years (2-3 times the average global rate of 0.15-0.20 °C per decade, Thompson et al., 2000; Xu et al., 2008; Luo et al., 2014), glaciers here retreated ~17% of coverage from 1980-2010 and 8894 km^2 from 2001-2015, mainly in the southern HTP (Qiu, 2010; Wang et al., 2019). It has been estimated that glaciers in HTP release 12.7-13.2 Gg C yr^{-1}, of which ~5.7 Gg C yr^{-1} is DOC (Yan et al., 2016; Liu et al., 2016). Meanwhile, the HTP contains three quarters of alpine permafrost (primarily discontinuous) in the North Hemisphere (Zhang et al., 2000, 2008). Permafrost area is ~1.06×10^6 km^2 (~40% of land surface of the HTP) containing and estimated 17.1 Pg organic carbon (Zou et al., 2017; Zhao et al., 2018a, 2018b). The active layer of permafrost here has deepened from 0.15 to 0.50 m between 1996-2001 (Yang et al., 2010). Moreover, land cover changes are obvious on the HTP, toward more grassland and permafrost degradation, deforestation, agricultural cropland expansion, urbanization, and desertification at a rate of ~1.8% increase per year (Zeng et al., 2003; Wang et al., 2008; Cui and Graf, 2009; Yang et al., 2010). About one-fifth of permafrost on the HTP has undergone degradation as well as erosion of thawed permafrost by waters from the numerous lakes and large rivers running across the plateau (Yang et al., 2010; Ma et al., 2018). In addition, black soot pollution and dust storm occurrence from local and distant origins have caught increasing scientific attention (Newton, 2007; Qiu, 2008; Xu et al., 2009; Li et al., 2016a; Chen et al., 2019). Tibetan dust bowl and black carbon are found to advance and intensify Indian summer monsoon (Lau et al., 2006). Most of the major rivers on the plateau are located in the central, eastern, and southeastern parts of the HTP.

Despite of the pivotal roles of the riverine DOM in the HTP, the comprehensive controls on the riverine DOM quantity and quality are still poorly understood there. Several prior studies have focused on the bulk DOC or optical and molecular fingerprints in glaciers or glacier- or permafrost-fed streams (Spencer et al., 2014; Wang et al., 2018; Chen et al., 2019). However, the HTP spans a vast mountainous highland with heterogeneous climate, land cover, biome, and human activities, it is crucial to investigate the major controls of riverine DOM quantity and quality across the HTP for climatic and biogeochemical modeling and suitable and sustainable management.

The main objectives of this study are three-fold: (1) study the characteristics of DOM in the major alpine rivers across the Tibetan Plateau by measuring bulk DOC concentration, 3D fluorescent excitation-emission matrix coupled with parallel factor analysis (EEM-PARAFAC), ultraviolet-visible (UV–Vis), and ultrahigh resolution Fourier transform ion cyclotron resonance mass spectrometry (FT-ICR MS); (2) investigate

dominant sources of riverine DOM via studying potential endmembers such as glacier meltwater, precipitation, vegetation, and sediment; (3) disentangle the principal controls (such as land cover, climate, human activities) on the quantity and quality of DOM in the alpine rivers from the HTP in monsoon season.

2. Methods

2.1. Site description

A constellation of jewel-toned alpine lakes and clear to yellowish alpine rivers are interspersed on the Tibetan Plateau. There are six major east-west tectonic blocks formed on the HTP: Qilian Block, Kunlun-Qaidam Block, Songpan-Ganzi Block in the north, Qiangtang Block in the central region, and Lhasa Block and Himalaya Block in the South (Yin and Harrison, 2000). The Yangtze River and Yarlung Zangbo River run along the sutures between the Qiangtang Block and Lhasa Block, and between the Himalaya Block and Lhasa Block, respectively. Vegetation on the HTP is dominated by alpine grassland (~70% in the study area, Table S1). The Tibetan Plateau hosts the world's largest pastoral alpine ecosystem (3000–6000 m a.s.l.) spanning an area of 450,000 km^2 which features a large and durable rhizosphere (Miehe et al., 2019). The alpine grassland can be categorized into three types: swamp meadow (dominated by *Kobresia tibetica*), alpine meadow (dominated by *Kobresia pygmaea* and *Kobresia humilis*) at the wet end of the central and eastern HTP, and alpine steppe (dominated by *Stipa purpurea* and *Carex moorcroftii*) at the dry part of the northern and western HTP (Zhang et al., 1988). A cluster of alpine forest sits in the southeastern HTP where the warm Indian monsoon corridor is located. The Taklimakan Desert is located to the north and the Gobi Desert to the northeast of the HTP (Fig. 1). There is an increasing gradient of precipitation and vegetation from northwest to southeast, with intensive Indian monsoon storms in southeast HTP (~1000-1500 mm yr^{-1} with > 70% in summer, Table S1; Fig. 2) while dry climate (<100 mm yr^{-1}) is found in the western part (Tong et al., 2014; Wang et al., 2016; Zou et al., 2017). In contrast, there is a general decreasing gradient of airborne dust events from northwestern to southeastern HTP (Kang et al., 2016; Li et al., 2016b).

The major alpine rivers on the Tibetan plateau include Yangtze River (Chang River, YT), Yellow River (Huang River, YR), Mekong River (named Lancang River at upstream, MR), Salween River (named Nu River at upstream, SR), and Yarlung Zangbo River (upstream of Brahmaputra River, YZ, Figs. 1 and S1). The former three drain into the Pacific Ocean while the latter two into the Indian Ocean. The Yangtze River is the third longest river in the world and drains approximately one-fifth of China's continental area. The Yellow River is one of the longest rivers in the world and is well known for its high sediment load in the mid- to lower reaches. Mekong River is also one of the ten largest rivers in the world by water and sediment discharge which mostly runs in deep gorges upstream. Inceptisols cover 36% of the upper Yangtze River and 50% of the upper Yellow River (Wu and Huh, 2007). The inorganic water chemistry of the Tibetan rivers is dominated by weathering of carbonates and evaporites. The Na^+, SO_4^{2-}, and Cl^- are high in central and eastern HTP while it is HCO_3^--Ca^{2+} type in the southern region (Qu et al., 2019).

2.2. Sampling

Surface waters from main stems and tributaries of the above-mentioned five alpine rivers, three glacier meltwaters, a precipitation

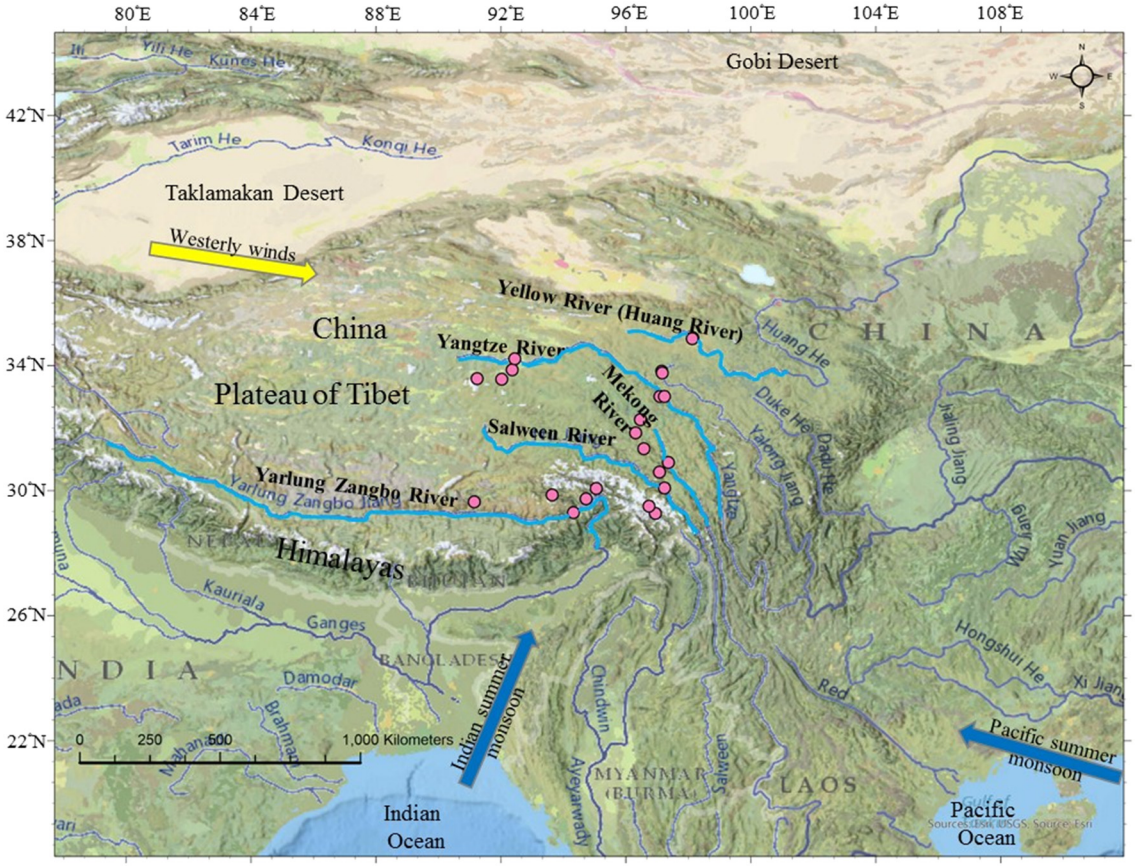

Fig. 1. Map of sampling sites of the main stems (highlighted in light blue) and tributaries of Tibetan major rivers in July 2018. Names of five rivers: Yangtze River (Chang), Yellow River (Huang), Mekong River (Lancang), Yarlung Zangbo River (Brahmaputra), Salween River (Nu). White patches are glaciers. (For interpretation of the references to color in this figure legend, the reader is referred to the web version of this article.)

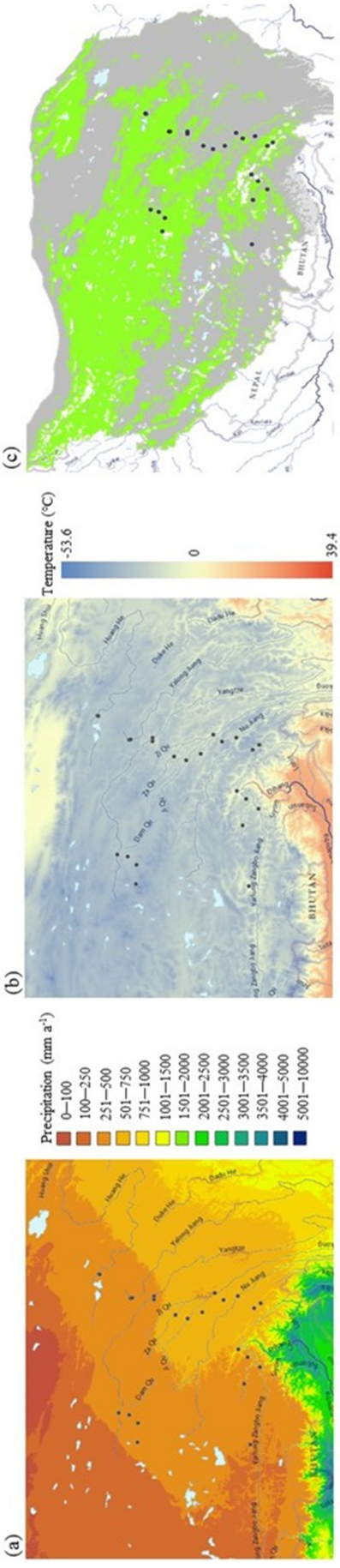

Fig. 2. (a) Annual precipitation distribution. (b) Mean July land temperature. (c) Distribution of permafrost (green color). Maps a, b, and c produced using ArcGIS (Esri, USA). Permafrost layer in (c) is from literature (Zou et al., 2017). (For interpretation of the references to color in this figure legend, the reader is referred to the web version of this article.)

event, sediments from four representative rivers, and a dominant grass species, namely *Kobresia pygmaea,* were collected in July 2018 during the peak of the monsoon season when stark spatial climatic variations on the HTP are expected (Fig. 1, Table S2). The sampling sites are representative of different climatic and land cover regimes (Fig. 2). Surface waters, glacier meltwaters, and surface sediments were collected with pre-cleaned Nalgene bottles. One precipitation sample was collected directly with a bottle when there was a sleet event in the three-river headwater region. Green above-ground grass (*Kobresia pygmaea)* was put into a pre-cleaned zip lock bag. All samples were stored in an ice box immediately after collection and during transportation to the laboratory. The grass sample was rinsed with Milli-Q water in the laboratory before the leaching experiment. Grass (~2 g L^{-1}) and sediment (~500 g L^{-1}) were leached with Milli-Q water for 24 h in the dark at room temperature (~25 °C). Electrical conductivity (EC) and pH were measured with a handheld multi-parameter water quality meter (ProDSS, YSI Inc., USA). All samples and leachates were filtered with 0.45 μm pre-rinsed cellulose filters (Millipore, USA) and then stored in a refrigerator (~3 °C) until further analysis.

2.3. DOC, UV–Vis, EEM-PARAFAC analyses

DOC concentrations were measured using a TOC-V WP total organic carbon analyzer (Shimadzu, Japan). Samples were acidified before measurement to purge inorganic carbon. Therefore, measured non-purgeable organic carbon (NPOC) equals to DOC. UV–Visible scans and EEMs were measured simultaneously with an Aqualog spectrometer (Horiba Scientific, Japan) between 240-500 nm for excitation (Ex) at 1 nm steps and 244-825 for emission (Em) at a 1.17 nm pixel. The integration time was set as 1 s. Charge-coupled device (CCD) detector gain was set as medium. Milli-Q water blank subtraction, inner filter effect correction, Rayleigh scatter cutting, and Raman unit (RU) normalization were conducted automatically on the platform of the Aqualog instrument software. PARAFAC analysis was conducted in MATLAB R2019a using DOMFluor toolbox. The number of EEMs was 58 and 4 components were identified (Fig. 3b). Since a larger EEMs dataset is helpful to robustly identify more components, we incorporated a prior riverine dataset from the HTP (Fig. 3c, Chen et al., 2019) to get to a total of 100 EEMs. Five PARAFAC components, including a photoproduct/photorefractory component $C_{<260/435}$, were identified (Fig. 3a). Associated optical indicators of specific absorption coefficient a^*_{254}, slope ratio (S_R), fluorescence index (FI), biological index (BIX), and humification index (HIX), proxies for aromaticity, molecular weight, fulvic acids sources, recent biological activities, and degree of humification, were calculated as described elsewhere (Weishaar et al., 2003; Helms et al., 2008; McKnight et al., 2001; Huguet et al., 2009; Zsolnay et al., 1999). The optical methods here can only observe optically actively chromophores (by UV–Vis) and fluorophores (by EEMs), respectively.

2.4. SPE pre-treatment and FT-ICR MS measurement

The solid phase extraction (SPE) was carried out using PPL cartridges (BondElut,

Agilent Inc.) as detailed elsewhere (Chen et al., 2016), with adjustment of sample volume based on DOC levels to ensure a similar load of organic carbon added to each PPL cartridge (Spencer et al., 2014). About 120 μg-C (for representative riverine samples from the Yangtze River, the Yellow River, and the Mekong River) target organic carbon loads (assuming a DOC extraction efficiency of 65%) were performed. Loaded PPL cartridges were dried with ultrapure N_2 (>99.999%) and residual HCl added for sample acidification was driven out completely. DOM was eluted with 1 ml of methanol. The FT-ICR MS measurements were performed using a 9.4-T instrument (in negative ion mode) housed in the National High Magnetic Field Laboratory in Florida, USA in absorption mode (Xian et al., 2010; Kaiser et al., 2011) and calibrated with a "walking" calibration based on highly abundant homologous

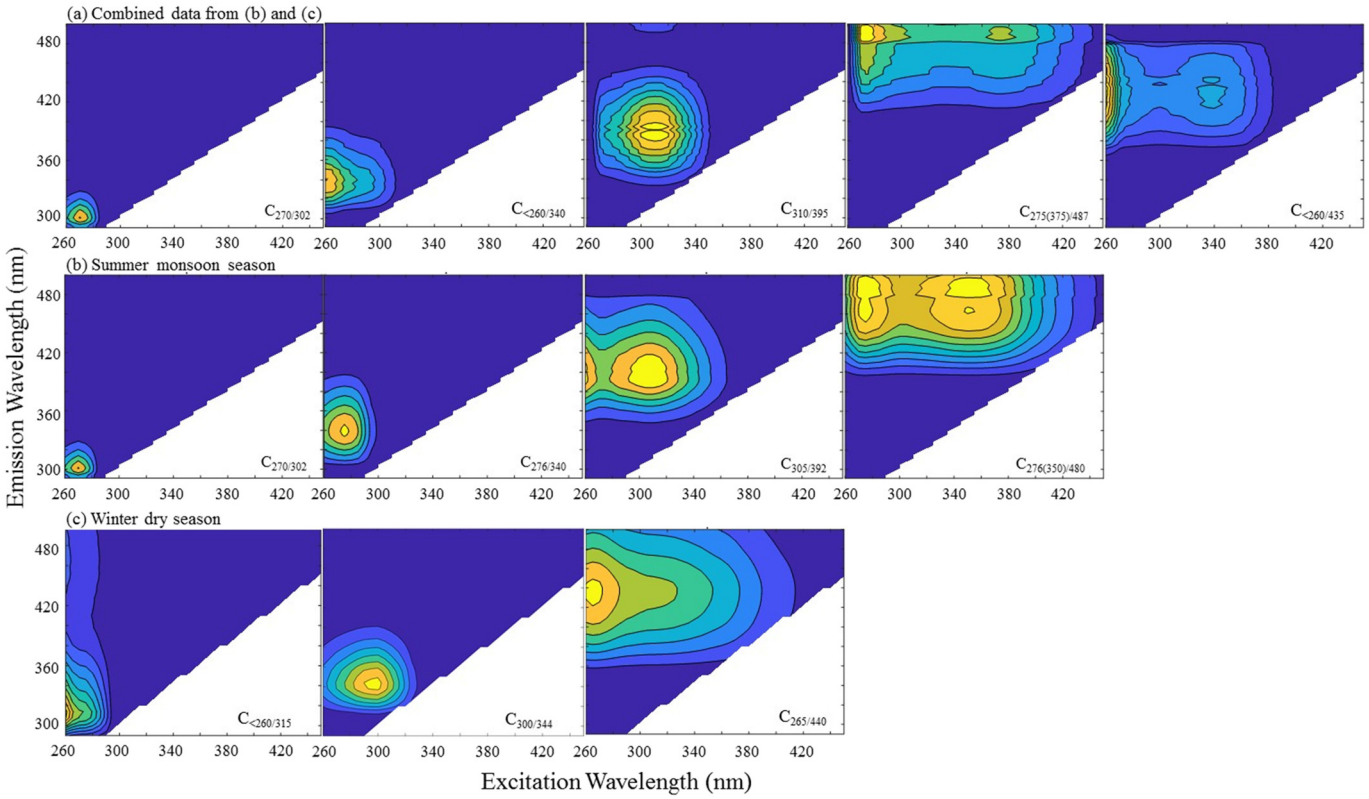

Fig. 3. Contour plots of identified EEM-PARAFAC components at major Tibetan rivers for (a) combined data from summer and winter, (b) summer monsoon season, and (c) southern glacier-fed streams in winter non-monsoon season (Chen et al., 2019). Bigger dataset is helpful to identify a photoproduct/photorefractory component $C_{<260/435}$ as seen from (a).

oxygen series (Savory et al., 2011). Mass spectral peaks with signal magnitude greater than six times the baseline root-mean-square noise level were exported to an excel sheet for elemental composition assignment. Formulae were assigned using a browser-based software (Leefmann et al., 2019). Library "02 NOM" was applied with $200 < m/z < 700$. The elemental combination of $^{12}C_{0-\infty}{}^{1}H_{0-\infty}{}^{16}O_{0-\infty}{}^{14}N_{0-5}{}^{32}S_{0-3}$ was applied. Mass error threshold was set at ≤1 ppm. Analytical filter (remove blank, surfactants, and formula not verified by ^{13}C, ^{34}S, and ^{15}N isotopes) and ratio filter ($O/C \le 1.2$, $0.3 \le H/C \le 2.3$) were also applied. Assigned molecular formulas were categorized into aliphatics ($O/C < 0.9$, $H/C > 1.5$, $N = 0$), peptides ($O/C < 0.9$, $H/C > 1.5$, $N > 0$), highly unsaturated ($AI_m < 0.5$, $H/C \le 1.5$), polyphenols ($0.67 > AI_m > 0.5$), and condensed aromatics ($AI_m \ge 0.67$) (Spencer et al., 2014).

3. Results and discussion

3.1. River water chemistry and DOM optical characteristics in monsoon season

The average pH of surface waters from the alpine rivers was 8.0-8.7, while pH for glacier meltwaters and the grass leachate was 7.9 ± 0.7 and 7.2 respectively (Table 1). The average electrical conductivity (EC) of riverine surface waters ranged from 94 to 972 μS cm^{-1}, with Yangtze and Yellow River's at the higher end, while the Yarlung Zangbo River was at the lower end, even lower than that of glaciers (110 μS cm^{-1}). Bulk DOC concentrations of river waters varied widely from 0.9 to 20.7 mg-C L^{-1}. DOC levels at one site of the Yangtze River (YT4) and one site of the Yellow River (YR1) were exceptionally high (>20 mg-C L^{-1}). This may be partly related to the inputs from in situ algal primary productivity in relatively stagnant waters in the headwater regions of these two large rivers. Relatively high S_R and FI while low a^*_{254} levels support the explanation above (Table 1). Similar to EC, DOC concentrations from the Yellow River and Yangtze River were 1–2 orders of magnitude higher than that in the Yarlung Zangbo River.

For UV–Visible properties, mean absorption coefficient of chromophoric DOM (CDOM) at 254 nm and 350 nm (i.e., a_{254} and a_{350}) for river waters ranged between 5.0-11.5 m^{-1} and 0.9-2.0 m^{-1}, comparable to those observed on the HTP previously (Gao et al., 2019). Average values of specific absorption coefficient a^*_{254}, an indicator of CDOM aromaticity, varied from as low as 0.4 m^2 g^{-1} at the Yangtze River to 7.9 m^2 g^{-1} at the Yarlung Zangbo River, a trend generally opposite to that of DOC concentration. The extremely low a^*_{254} in the Yangtze and Yellow Rivers reflects low aromatic DOM inputs and/or highly photodegraded DOM characteristics especially in the dry northern and central HTP where solar irradiation is very strong, consistent with a prior observation for riverine waters from the HTP (Chen et al., 2019). Slope Ratio (S_R), a proxy for molecular weight of CDOM, ranged from 4.0 to 10.5 with Yellow River at the higher end and Yarlung Zangbo River at the lower end, implying larger molecular weight of CDOM from alpine rivers on the southern HTP. This is consistent with the higher aromaticity indicator of a^*_{254} in the southern rivers.

As for fluorescent DOM (FDOM), fluorescence index (FI) was ~1.3-1.4, suggesting primarily terrestrial sources of FDOM in Tibetan rivers in the monsoon season (McKnight et al., 2001). Mean BIX and HIX were 0.7-1.0 and 0.7-1.8, respectively. As mentioned above, EEM-PARAFC modeling identified five components after combining EEMs from a previous study in the HTP: two protein-like $C_{270/302}$ and $C_{<260/340}$, one microbial humic-like $C_{310/395}$, and two terrestrial humic-like $C_{275(375)/487}$ and $C_{<260/435}$ (Table 1; Fig. 3a). Average intensities of $C_{270/302}$ and $C_{<260/340}$ ranged between 0.71-1.23 RU and 0.10-0.17 RU, respectively. $C_{310/395}$ varied from 0.08 ± 0.05 RU at the Yarlung Zangbo River and 0.11 ± 0.00 RU at the Yangtze and Salween Rivers. $C_{275(375)/487}$ and $C_{<260/435}$ ranged between 0.10-0.18 RU and 0.15-0.29 RU, respectively. For relative contribution of

Table 1
Summary of water chemistry and DOM characteristics of surface water samples from Tibetan rivers and lakes.

Item	Unit	Yellow	Yangtze	Mekong	Salween	YZ	YZ (winter)[a]	Glacier	Sleet	Sediment	Grass
		$n = 2$	$n = 6$	$n = 4$	n = 2	n = 6	$n = 7$	$n = 3$	$n = 1$	n = 4	n = 1
pH		8.7 ± 0.2	8.3 ± 0.3	8.3 ± 0.4	8.2 ± 0.2	8.0 ± 0.2	8.4 ± 0.1	7.9 ± 0.7	n/a	n/a	7.2
EC	$\mu S\ cm^{-1}$	658 ± 98	972 ± 775	343 ± 136	167 ± 79	94 ± 39	330 ± 82	110 ± 65	n/a	122 ± 58	11
DOC	$mg\text{-}C\ L^{-1}$	20.7 ± 10.1	14.2 ± 5.7	5.3 ± 2.8	1.5 ± 0.1	0.9 ± 0.5	0.5 ± 0.2	0.4 ± 0.0	1.4	4.8 ± 5.7	2.4
a_{254}	m^{-1}	11.5 ± 4.3	5.9 ± 5.2	5.0 ± 1.4	7.5 ± 1.5	6.5 ± 3.8	3.1 ± 0.9	1.6 ± 1.8	2.2	15.1 ± 6.9	15.8
a_{350}	m^{-1}	1.4 ± 0.3	1.3 ± 1.1	1.2 ± 0.3	2.0 ± 0.6	2.0 ± 1.0	0.9 ± 0.5	0.5 ± 0.5	0.5	4.6 ± 1.8	6.5
a^*_{254}	$m^2\ g^{-1}$	0.6 ± 0.1	0.4 ± 0.3	1.6 ± 1.6	4.9 ± 0.8	7.9 ± 1.1	5.1 ± 7.5	4.3 ± 4.4	1.5	7.9 ± 8.6	6.6
S_R		10.5 ± 2.8	5.7 ± 0.9	5.2 ± 0.3	4.3 ± 0.2	4.0 ± 0.4	4.8 ± 1.0	7.9 ± 2.4	9.6	3.6 ± 0.5	2.4
FI		1.4 ± 0.1	1.4 ± 0.1	1.4 ± 0.1	1.3 ± 0.0	1.3 ± 0.1	1.7 ± 0.0	1.6 ± 0.4	1.2	1.3 ± 0.0	1.2
BIX		0.9 ± 0.1	0.8 ± 0	0.9 ± 0.1	0.7 ± 0.1	1.0 ± 0.5	1.0 ± 0.2	0.7 ± 0.3	1.1	0.7 ± 0.0	0.8
HIX		1.8 ± 1.8	1.2 ± 0.8	0.8 ± 0.2	1.1 ± 0.2	0.7 ± 0.5	2.2 ± 1.3	0.2 ± 0.1	0.2	1.8 ± 1.1	0.6
$C_{270/302}$	RU	0.71 ± 0.89	0.87 ± 0.27	1.23 ± 0.10	1.19 ± 0.05	1.05 ± 0.14	0.02 ± 0.03	0.117 ± 0.014	1.10	0.41 ± 0.14	0.25
$C_{<260/340}$	RU	0.16 ± 0.10	0.10 ± 0.05	0.13 ± 0.05	0.14 ± 0.02	0.17 ± 0.13	0.09 ± 0.05	0.006 ± 0.001	0.12	0.68 ± 0.06	0.66
$C_{310/395}$	RU	0.11 ± 0.00	0.10 ± 0.09	0.10 ± 0.04	0.11 ± 0.00	0.08 ± 0.05	0.06 ± 0.01	0.001 ± 0.001	0.04	0.20 ± 0.14	0.20
$C_{(275)375/487}$	RU	0.11 ± 0.00	0.13 ± 0.12	0.12 ± 0.04	0.18 ± 0.02	0.10 ± 0.07	0.05 ± 0.01	0.001 ± 0.001	0.02	0.24 ± 0.24	0.16
$C_{<260/435}$	RU	0.23 ± 0.02	0.24 ± 0.23	0.21 ± 0.07	0.29 ± 0.04	0.15 ± 0.11	0.09 ± 0.02	0.003 ± 0.002	0.03	1.83 ± 0.40	0.25
$C_{270/302}$	%	40 ± 38	64 ± 17	69 ± 6	62 ± 2	69 ± 14	8 ± 8	91 ± 4	84	53 ± 20	16
$C_{<260/340}$	%	13 ± 2	7 ± 1	7 ± 2	8 ± 1	10 ± 6	27 ± 12	5 ± 1	9	7 ± 1	43
$C_{310/395}$	%	11 ± 8	7 ± 3	5 ± 1	6 ± 0	5 ± 3	20 ± 3	1 ± 1	3	7 ± 3	13
$C_{(275)375/487}$	%	12 ± 9	8 ± 4	7 ± 1	9 ± 1	6 ± 4	15 ± 3	1 ± 1	2	12 ± 6	11
$C_{<260/435}$	%	24 ± 19	15 ± 8	12 ± 2	15 ± 2	9 ± 7	30 ± 6	2 ± 2	2	21 ± 10	17

YZ: Yarlung Zangbo River.
[a] Data re-processed from Chen et al. (2019).

PARAFAC components, tyrosine-like $C_{270/302}$ generally dominated with an average of 40-69%, followed by the photoproduct $C_{<260/435}$ (9-24%).

3.2. Molecular signatures of DOM in alpine rivers from the HTP: evidences of black soot pollution

Thousands of molecular formulae (2993-5548) have been obtained from FT-ICR MS measurements (Table 2), which largely fell into the categories of highly unsaturated (47-64%), followed by polyphenols (17-20%) and condensed aromatics (14-21%) in the van Krevelen diagrams (Fig. 4; Figs. S2–S3). The percentages of condensed aromatics here are significantly higher than the world's average of ~11% even in the wet season (Jaffé et al., 2013) but lower than those in the dry season when about one-third was observed (Chen et al., 2019). These observations are consistent with black soot pollution on the previously thought pristine plateau. The HTP is surrounded by hotspots of air pollution via long-distance transport from East and South Asia and also local sources of yak dung and biomass combustion (Qiu, 2008; Li et al., 2016a). Aliphatics and peptides only accounted for 3-11% and 2%, respectively. Dissolved black nitrogen (DBN) generally dominated condensed aromatics (44-71%), with a significant amount of DBN containing multiple nitrogen which has been found to be produced by incomplete combustion of grassy biomass (Fig. 4, Knicker, 2010). Weight-averaged (wa) m/z were 393-419. Double bond equivalent (DBE_{wa}) and modified aromatic index ($AI_{m,wa}$) were 11-12 and 0.32-0.37, respectively. $AI_{m,wa}$ was relatively higher in the southern rivers than those in the northern rivers, consistent with the trend of a^*_{254} for CDOM aromaticity proxy. S-containing formulae were up to 27% in the Yellow River as compared to 7-9% in other rivers. Likewise, N-containing formulae consisted of 46% in the Yellow River, higher than the 36-37% reported in other rivers. This may be partly related to algal inputs in the relatively stagnant water at the Yellow River source. Similar to condensed aromatics, percent of heteroatomic formulas is also much lower in monsoon season than those in non-monsoon season, suggesting impacts of precipitation in monsoon season.

Table 2
Weight-averaged (wa($\overline{M_w}$)) molecular characteristics of representative sites in Tibetan major rivers.

Items	Yellow River	Yangtze River	Mekong River	Yarlung Zangbo River[d]
Formula #	4415	2993	5548	1328–1891
m/z_{wa}	419	393	406	429–449
DBE_{wa}[a]	12	11	12	14–15
$AI_{m,\ wa}$[b]	0.32	0.36	0.37	0.50–0.60
H/C_{wa}	1.13	1.08	1.06	0.99–1.03
O/C_{wa}	0.41	0.47	0.41	0.17–0.21
N/C_{wa}	0.06	0.04	0.04	0.11–0.15
S/C_{wa}	0.024	0.008	0.008	0.05
CHO-only (%)	37	62	60	8–15
DOS (%)	27	7	9	58–72
DON (%)	46	36	37	61–83
Condensed aromatics (%, DBN%[c])	21(71)	14(53)	18(44)	33–38(91–99)
Polyphenols (%)	17	17	20	18–33
Highly unsaturated, O/C < 0.5 (%)	24	31	32	23–24
Highly unsaturated, O/C > 0.5 (%)	23	33	24	2–7
Aliphatics (%)	11	3	3	1–10
Peptides (%)	2	2	2	3–8

[a] DBE (double bond equivalent) = 1 + 0.5(2C-H + N) (Koch et al., 2005).
[b] AI_m (modified aromatic index) = (1 + C-0.5O-S-0.5H)/(C-0.5O-S-N-P) (Koch and Dittmar, 2006).
[c] DBN: dissolved black nitrogen.
[d] Contains high percent of condensed aromatics (Chen et al., 2019).

3.3. Temporal variations of surface water DOM in Tibetan rivers

DOC concentrations were higher in the summer monsoon season than in the winter season in the Yarlung Zangbo River (0.9 ± 0.5 vs. 0.5 ± 0.2 $mg\text{-}C\ L^{-1}$, Table 1). Likewise, CDOM a_{254} and a_{350} and FDOM PARAFAC component intensities were also higher in magnitude in the monsoon season. FI values of 1.3 ± 0.1 indicated a more terrestrial source of fulvic acids in the monsoon season as compared to more microbial and algal sources in winter with FI values of 1.7 ± 0.0 (McKnight et al., 2001). These observations are consistent with the different dominant river waters in summer vs. winter. Glacier meltwater and groundwater usually dominates the inputs of stream flow across alpine basins during winter (Chen et al., 2019; Malard et al., 1999, 2006). In winter, groundwater is recharged at high elevation primarily by glacier/snow meltwaters. In contrast, precipitation, including rainfall and sleet, contributes heavily to river waters in summer, especially in the southeastern HTP along the Indian monsoon corridor. DOC

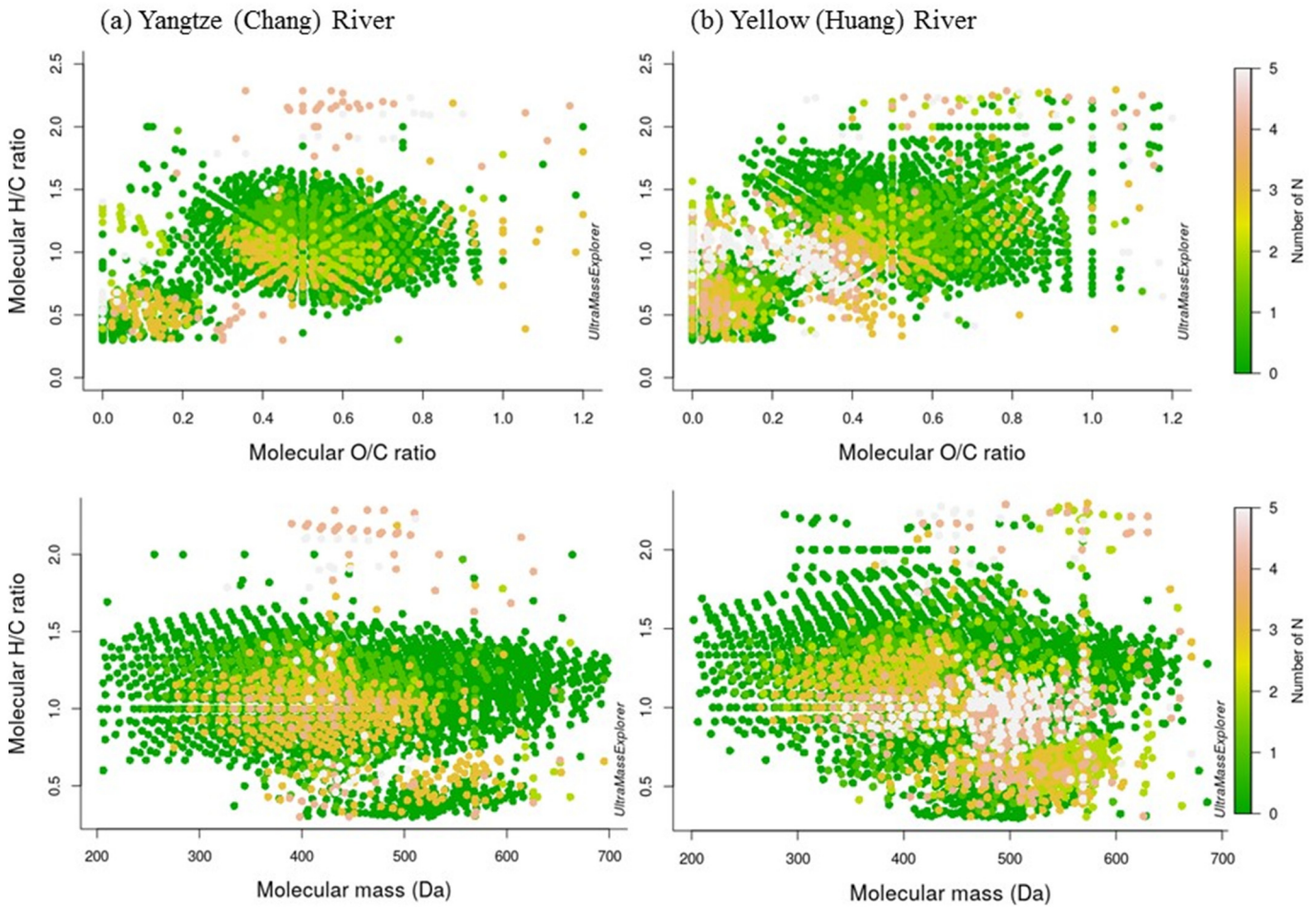

Fig. 4. Examples of van Krevelen diagrams (upper panel) and the plots of the H/C ratios vs. the *m/z* ratios (lower panel) of the formula distribution for surface waters from major rivers in the Himalayan-Tibetan Plateau. N-containing formulas mainly fall into categories of condensed aromatics ($AI_m \geq 0.67$), polyphenols ($0.67 > AI_m > 0.5$), and peptides (O/C < 0.9, H/C > 1.5, $N > 0$).

concentration in a sleet sample was 1.4 mg-C L^{-1}, much higher than those in glacier meltwaters of 0.4 mg-C L^{-1} (Table 1), consistent with observations in prior studies (Spencer et al., 2014; Li et al., 2017). Glacial waters are more of microbial and/or algal in character, while precipitation and catchment runoff can flush more terrestrial-derived DOM into fluvial systems (Fig. 3, Lafrenière and Sharp, 2004; Wilson et al., 2016).

3.4. Spatial trends of riverine DOM with latitude caused by climatic gradients

Interestingly, there is a positive correlation between DOC and latitude ($r = 0.88$, $p < 0.0001$) and an inverse correlation between a^*_{254} and latitude ($r = 0.88$, $p < 0.0001$), indicative of a general trend of higher levels of DOM quantity in the northern rivers while higher CDOM aromaticity in the southern counterparts (Fig. 5a-b). However, such correlations with longitude are not observed. DOC levels decreased exponentially with a^*_{254} with a rate constant of −0.9 ($r = 0.77$, $p < 0.0001$, Fig. 6a). Furthermore, principal component analysis (PCA, performed in R software with vegan package) also displayed clear clusters of samples from different alpine watersheds, and principal component 2 (PC2) was largely ordered from northern to southern rivers along PC2 axis's positive to negative direction (Fig. 7).

These spatial trends can be primarily explained by a decreasing gradient of dust events and an increasing gradient of precipitation and vegetation from the northwestern to southeastern plateau (Fig. 2; Fig. 5). There is approximately 800 Tg yr^{-1} aeolian dust emission from the vast semi-arid and arid Taklimakan and Gobi deserts in NW China (Zhang et al., 1997). DOC concentrations were significantly correlated to electrical conductivity (EC, $r = 0.53$, $p < 0.05$, Fig. 6b) in this study, in line with a trend of positive relationships between DOC and EC, total dissolved solids (TDS), as well as insoluble particulate carbon (IPC) in Tibetan rivers and glaciers (Li et al., 2016b; Chen et al., 2019). Mineral and soil dusts are believed to be the dominant sources of DOM in glaciers and snow over the Tibetan Plateau, with a decreasing trend from north to south (Li et al., 2016b; Thapa et al., 2020). The correlation between DOC and EC here supports that soil and mineral dusts are potentially the dominant sources of DOM in rivers as well. As we can see from the map (Fig. 1), several large deserts (e.g., the Taklamakan Desert and the Gobi Desert) border with the HTP to the north and northwest. Desertification due to overgrazing is also a widespread phenomenon in the northern HTP, including the upper reaches of the Yellow River (Zeng et al., 2003). As such, frequent dust events, including dust storm (visibility <1 km), blowing dust (1 km < visibility <10 km, and floating dust (visibility >10 km), can occur from the deserts and bareland surface in the northwestern HTP driven by the middle latitude westerly jet (Kang et al., 2016). Dust events are active in winter to spring (December to May) when the westerly wind dominates the air circulation over the HTP. Summertime dust aerosol plumes originated from the northern slopes of the HTP and nearby deserts are also detected (Huang et al., 2007). Dust events have decreased since the 1970s due to a weakened surface wind speed. Local sources of dust dominate in winter and spring while distant sources prevail in summer and autumn (Kang et al., 2016). Furthermore, a concentration effect

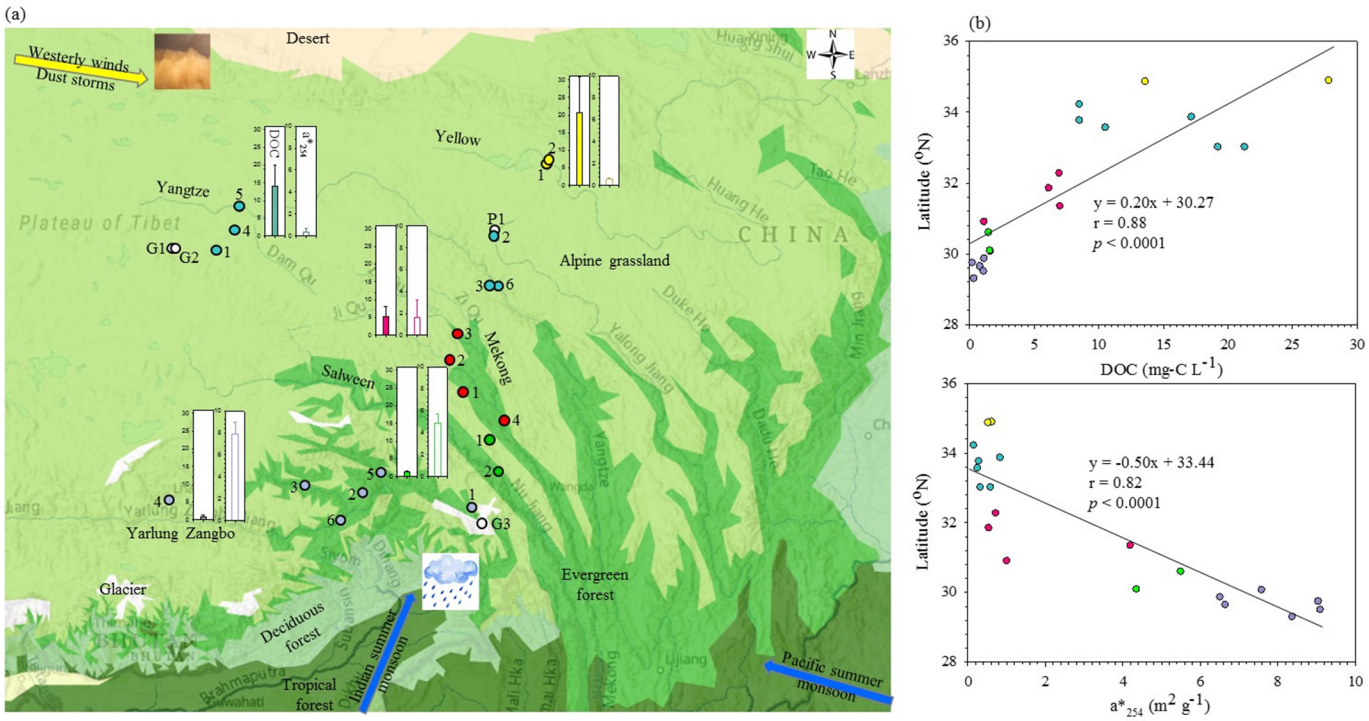

Fig. 5. General increasing trend of DOC with latitude and the opposite trend of specific absorption coefficient a^*_{254} (CDOM aromaticity index) observed in the Tibetan Plateau. Map (a) with biomes produced using ArcGIS Pro (Esri). Numbers beside the symbols correspond to site numbering in Fig. 6 and Table S2. Arrow sizes indicate direction only and are not proportional to fluxes.

caused by evaporation in arid and semi-arid regions with high wind speed in the northern HTP can also contribute to higher DOC levels there (Liu et al., 2011).

In contrast, frequent summer storms occur in the southeastern HTP, where the Indian monsoon can penetrate the Himalayas and form a monsoon corridor (Fig. 2, Fig. 5). DOC concentrations (0.9 ± 0.5 mg-C L^{-1}, Table 1) in southern Yarlung Zangbo River were at similar levels as in precipitation over the HTP at 0.8-1.0 mg-C L^{-1} (Li et al., 2017), implying extensive dilution by rainwaters. Gradients of much heavier precipitation and lighter dust load from NW to SE would render a gradient of lower DOC but higher a^*_{254} from NW to SE across major Tibetan rivers, given that hydrological high-flow events can flush more high aromaticity DOM from terrestrial soil and plant debris (Wilson et al., 2016; Chen et al., 2020). The weight-averaged AI_m data from FT-ICR MS measurements corroborated this trend (Table 2).

3.5. Effects of land cover: glacier vs. terrestrial vegetation and soil

Catchment runoff regime can be shifted as a function of the degree of glaciation, vegetation, edaphic ecotype, and permafrost cover. Based on PCA graph (Fig. 7), we saw a general trend of small tributaries closer to glaciers distributed on the left side of PC1(48%) axis which was controlled by glacier/snow-derived DOM sources, while most river main stems and tributaries with larger catchment basins distributed on the right side of the PC1 axis indicative of DOM sources from sediment and grass leachates (stream types available in Table S2). This can be explained by more glacier meltwater inputs in lower-order proglacial headwaters and small streams closer to glaciers, while more terrestrial soil and higher plant DOM flushed into main stems and tributaries with large drainage basins. From the loading plot of the PCA, relative abundance of tyrosine-like fluorescence $\%C_{270/302}$ distributed on the

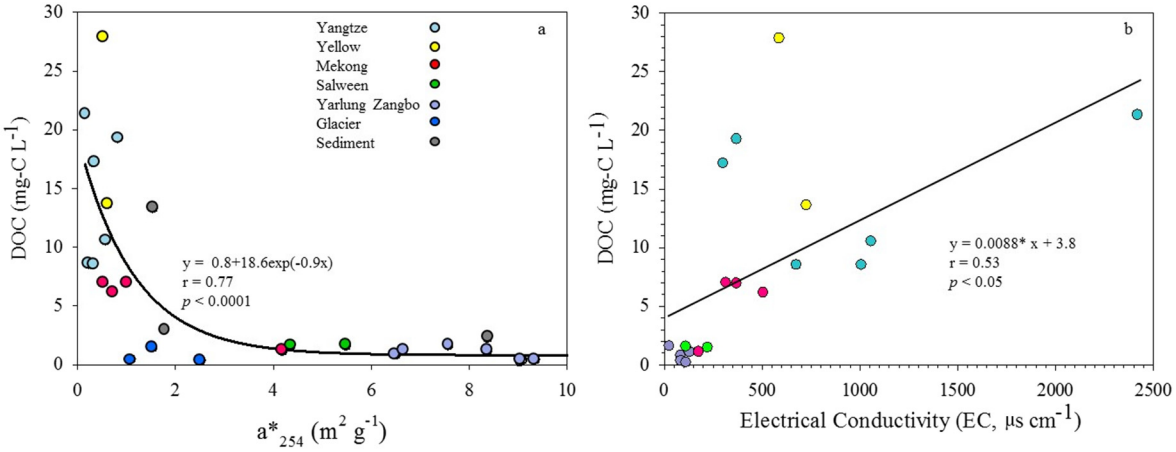

Fig. 6. First-order exponential decay of DOC with a^*_{254} (a) and positive correlation between DOC and EC (b).

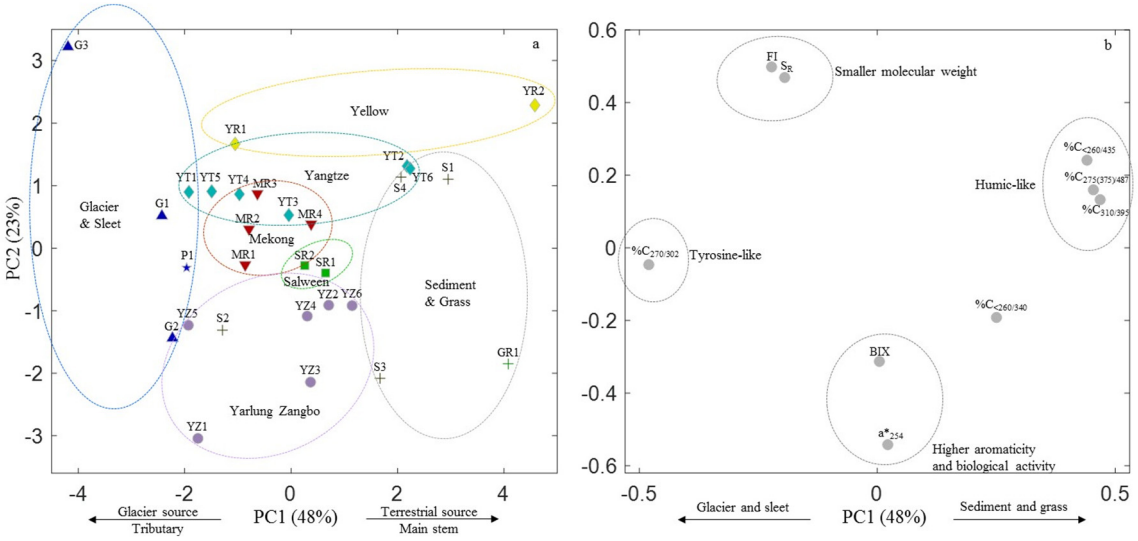

Fig. 7. Principal component analysis (PCA) based on DOM quality parameters for river surface waters, glacier meltwaters (G), precipitation (P), sediment (S) and grass (GR) leachates from the HTP. YT, YR, YZ, MR, and SR denote Yangtze River, Yellow River, Yarlung Zangbo River, Mekong River, and Salween River, respectively. River types can be found in Table S2. YR2, YT6, MR4, SR2, and YZ6 are main stems.

glacier meltwater side while three humic-like components clustered on the sediment and grass leachates side. This observation is consistent with a prior finding of higher evasion rates of CO_2 in tributaries than those in mainstreams (Qu et al., 2017), due to the higher bioavailability of glacial DOM than terrestrial-derived DOM. Glacier meltwaters usually contain low DOC concentrations (0.4 ± 0.0 mg-C L^{-1}) dominated by tyrosine-like fluorescence ($91 \pm 4\%$, Table 1). However, glacier DOM can be derived from multiple sources, including in situ primary production as well as local and distant deposition from terrestrial and anthropogenic sources (Stubbins et al., 2012; Hood et al., 2015). Cryoconite holes, colonized by an array of microorganisms (e.g., algae, bacteria, viruses), cover ~0.1-10% of the surface area of glaciers. They have high microbial activity despite low temperature. For example, in situ primary productivity in cryoconite holes can fix ~64 Gg-C yr^{-1} outside of Antarctica (Anesio et al., 2009). It was estimated that glacier meltwater contributes >50% of the total runoff increase in the Yarlung Zangbo River (Su et al., 2016). Therefore, more glacier-derived DOM will be expected in the southern Yarlung Zangbo River.

Permafrost-dominated watersheds potentially underlain with peat tend to have high DOC and a^*_{254} (Petrone et al., 2006; Balcarczyk et al., 2009). However, compared to soil and mineral dust, permafrost seems not be a major contributor of DOM to the rivers because of the lower aromaticity proxy of a^*_{254} in the northern and central Tibetan rivers where permafrost coverage is higher than southern rivers (Fig. 2, Table S1). Another possibility of low a^*_{254} is permafrost-derived DOM is removed quickly along the stream flow path via flocculation and/or degradation as observed previously (Wang et al., 2018). The PCA suggests smaller molecular weight DOM (i.e., higher S_R) in the northern rivers. Indeed, higher DOC levels in northern rivers are not contributed by optically active DOM as seen in Table 1. Nevertheless, higher-order rivers and main stems draining larger basin areas can receive more catchment runoff carrying terrestrial soil and higher plants-derived DOM.

3.6. Comparison of Tibetan DOM characteristics with alpine watersheds worldwide

It is well-known that all alpine rivers are affected by land cover of drainage basins and are responding to ongoing global glacier retreat and permafrost thaw. Other than this, alpine rivers on the HTP are also severely impacted by the special climate of frequent dust events in the north and center and intense monsoon storms in the southeast, as well as increasing anthropogenic activities. The multiple controls by climate, land cover, and humans bring unique spatial gradients and wide heterogeneity to riverine DOM quantity and quality on the HTP.

DOC concentrations from the Tibetan watersheds ranged widely from 0.2 to 37 mg-C L^{-1}, reflecting large variations in land cover, dust events, and precipitation across the HTP. The highest value was from a small alpine lake on the HTP (Chen et al., 2019), potentially caused by a concentration effect due to extensive evaporation under strong solar irradiation (Osburn et al., 2017). Similarly, DOM quantity and quality from global alpine watersheds also varied greatly, and was generally higher concentrations in basins affected by intense aeolian dust deposition and/or underlain with discontinuous permafrost, while lower in proglacial streams (Table 3). DOC concentrations in eastern Alp streams were 1.1-5.4 mg-C L^{-1}, as compared to ~0.1-11.8 mg-C L^{-1} from alpine watersheds in the Rocky Mountain range of North America (Mcknight et al., 1997; Hood et al., 2002, 2005; Lafrenière and Sharp, 2004; Fasching et al., 2016). Alpine streams in the Yukon of Canada showed DOC levels of ~1-7 mg-C L^{-1} (Shatilla and Carey, 2019). FI varied between 1.2 and 1.8 in the Tibetan Plateau, suggesting shifting algal/microbial, terrestrial, or a mix of DOM sources in different alpine watersheds. Huge variations of a^*_{254} on the HTP from 0.2 to 60 m^2 g^{-1} also corroborated this point. An extremely high maximum a^*_{254} value was observed in a glacier-fed stream at a high altitude of ~5200 m a.s.l. in the Himalayas (Chen et al., 2019), potentially caused by photo-induced production of Nature's sunscreen mycosporine-like amino acids (MAAs) by organisms (e.g., algae and bacteria) in response to strong solar irradiation at high altitude (Feng et al., 2016). It is apparent, DOC concentration, FI, and a^*_{254} all have the widest span on the HTP in comparison to other alpine watersheds. Indeed, the HTP has the highest mountain glaciers in the world and covers a vast area with varying climate condition (dust storm, monsoon storm, soot pollution), land cover (grassland, forest, glacier, desert, wetland, etc.), and seasonal trends (monsoon and non-monsoon seasons), which leads to unique gradients of DOM quantity and quality over the Tibetan Plateau and huge variation of DOM characteristics across the alpine waters.

4. Conclusion and environmental implications

Taken together, observed special climate (e.g., monsoon storm combined with dust events), land cover (i.e., glacier-studded, discontinuous permafrost, dominant grassland biome interspersed with forest and bareland), and intensified anthropogenic activities on the Tibetan Plateau explain the distribution of DOM

Table 3
Comparison of DOM parameters at the Himalayan-Tibetan Plateau (HTP) with those from other alpine watersheds.

Item	Location	Time	Altitude (m a.s.l.)	DOC (mg-C L^{-1})	FI	a^*_{254} (m^2 g^{-1})	$AI_{m,\ wa}$	Reference
Streams:								
Alpine	Central to southeastern HTP	Jul. 14–Jul. 20, 2018	~2000–5300	0.2–27.8	1.2–1.5	0.2–9.4	0.3–0.4	In this study
Glacier-fed	Southern HTP	Nov. 29–Dec. 9, 2017	~2000–5300	0.1–2.1	1.7–1.8	0.3–60	0.3–0.6	Chen et al., 2019
Underlain with permafrost	Northeastern HTP	Aug.–Oct., 2015–2016	~3000–4000	~2–14	–	~3–7	~0.4	Wang et al., 2018
Proglacial	Central HTP	–	~4500	0.3	–	1.3–1.4	–	Spencer et al., 2014
Alpine	Eastern Alps	May 2010–Aug. 2013	–	1.1–5.4	–	~1.5–7.0	–	Fasching et al., 2016
Alpine	Colorado Front Range	Spring–summer, 1999	~3500	~0.3–11.8	–	–	–	Hood et al., 2002
Underlain with permafrost	Yukon, Canada	Spring–winter, 2015–2016	~1300–2100	~1–7	~1.4–1.7	~5–12	–	Shatilla and Carey, 2019
Glacier-fed stream	Banff National Park, Canada	Spring–summer, 1998–2000	~2600	~0.1–1.1	1.5–1.7	–	–	Lafrenière and Sharp, 2004
Lakes:								
Alpine	Central to southeastern HTP	Jul. 17–Jul. 19, 2018	~4000	0.3–28	1.3–1.5	0.5–9.1	–	In this study
Alpine	Southern HTP	Nov. 29–Dec. 9, 2017	~4500	~4–37	1.4–1.5	0.2–0.6	–	Chen et al., 2019
Alpine	Colorado Front Range	Spring–summer,1999–2000	~3500	~0.5–2.6	~1.3–1.5	~3.5–9.2	–	Hood et al., 2005
Proglacial	Central HTP	–	~4500	3.1–4.6	–	1.5–1.6	–	Spencer et al., 2014
Alpine	Rocky Mountain National Park	Jul. 13–Aug. 11, 1993	~3300	~0.4–0.8	–	–	–	Mcknight et al., 1997

characteristics and dynamics from alpine rivers over the HTP. With condensed aromatics accounting for 14–21% in the monsoon season and about 33% in the non-monsoon season in the riverine DOM, anthropogenic footprints show that the HTP is no longer a pristine place as we previously thought. Trends of warming, glacier retreat, permafrost thawing, grassland degradation, increasing precipitation and vegetation in central and SE, and decreasing dust storms are expected to interplay intricately. Paradoxically, seemingly natural forcings, both land cover and climate, are affected by human activities as well. Overgrazing of grassland leads to more bareland, which will be exposed to wind to emit dust and soil. Fossil fuel and biomass combustion can also generate not only more greenhouse gas of CO_2, but also more black carbon aerosols, accelerating glacier melt and intensify Indian monsoon. As such, humans need to put forward a range of efforts from improved land management to mitigation of fossil fuel and biomass combustion for better environmental responses for sustainable alpine waters originated from the third pole.

CRediT authorship contribution statement

M.C. contributed to study design. M.C. collected the sample with help from C.L. and F.Y. M.C. did water quality, DOC, optical measurements, and SPE pre-treatments. A.M.M. did the FT-ICR MS measurements. M.C. processed the data and drafted the manuscript with comments from all other authors.

Declaration of competing interest

The authors declare no competing interest.

Acknowledgements

The authors are grateful for Rudolf Jaffe's insightful comments on an earlier version of this manuscript and Boris P. Koch's valuable help with UME. Thanks also go to Sydney F. Niles for assistance with FT-ICR MS data acquisition, Jiangcun Zewang for help with field sampling and Jennifer Rogers for help with SPE pre-treatment. This work was supported by a key discipline fund in environmental science and engineering and a special fund for science and technology from Guangdong Province, China and the second Tibetan Plateau Scientific Expedition and Research Program (STEP) (2019QZKK0605). FT-ICR MS measurements were performed at the Ion Cyclotron Resonance user facility at the National High Magnetic Field Laboratory, which is supported by the National Science Foundation Division of Chemistry and Division of Materials Research through Cooperative Agreement No. DMR-1644779* and the State of Florida.

Appendix A. Supplementary data

Supplementary data to this article can be found online at https://doi.org/10.1016/j.scitotenv.2020.142411.

References

Abbott, B.W., Jones, J.B., Schuur, E.A.G., Chapin Iii, F.S., Bowden, W.B., Bret-Harte, M.S., Epstein, H.E., Flannigan, M.D., Harms, T.K., Hollingsworth, T.N., Mack, M.C., McGuire, A.D., Natali, S.M., Rocha, A.V., Tank, S.E., Turetsky, M.R., Vonk, J.E., Wickland, K.P., Aiken, G.R., Alexander, H.D., Amon, R.M.W., Benscoter, B.W., Bergeron, Y., Bishop, K., Blarquez, O., Ben, B.-L., Breen, A.L., Buffam, I., Cai, Y., Carcaillet, C., Carey, S.K., Chen, J.M., Chen, H.Y.H., Christensen, T.R., Cooper, L.W., Cornelissen, J.H.C., de Groot, W.J., DeLuca, T.H., Dorrepaal, E., Fetcher, N., Finlay, J.C., Forbes, B.C., French, N.H.F., Gauthier, S., Girardin, M.P., Goetz, S.J., Goldammer, J.G., Gough, L., Grogan, P., Guo, L., Higuera, P.E., Hinzman, L., Hu, F.S., Hugelius, G., Jafarov, E.E., Jandt, R., Johnstone, J.F., Jan, K., Kasischke, E.S., Kattner, G., Kelly, R., Keuper, F., Kling, G.W., Kortelainen, P., Kouki, J., Kuhry, P., Laudon, H., Laurion, I., Macdonald, R.W., Mann, P.J., Martikainen, P.J., McClelland, J.W., Molau, U., Oberbauer, S.F., Olefeldt, D., Paré, D., Parisien, M.-A., Payette, S., Peng, C., Pokrovsky, O.S., Rastetter, E.B., Raymond, P.A., Raynolds, M.K., Rein, G., Reynolds, J.F., Robards, M., Rogers, B.M., Schädel, C., Schaefer, K., Schmidt, I.K., Shvidenko, A., Sky, J., Spencer, R.G.M., Starr, G., Striegl, R.G., Teisserenc, R., Tranvik, L.J., Virtanen, T., Welker, J.M., Zimov, S., 2016. Biomass offsets little or none of permafrost carbon release from soils, streams, and wildfire: an expert assessment. Environ. Res. Lett. 11 (3), 034014.

Anesio, A.M., Hodson, A.J., Fritz, A., Psenner, R., Sattler, B., 2009. High microbial activity on glaciers: importance to the global carbon cycle. Glob. Chang. Biol. 15 (4), 955–960.

Balcarczyk, K.L., Jones, J.B., Jaffe, R., Maie, N., 2009. Stream dissolved organic matter bioavailability and composition in watersheds underlain with discontinuous permafrost. Biogeochemistry 94 (3), 255–270.

Bianchi, T.S., 2011. The role of terrestrially derived organic carbon in the coastal ocean: a changing paradigm and the priming effect. Proc. Natl. Acad. Sci. 108 (49), 19473–19481.

Chen, M., Kim, S., Park, J.-E., Jung, H.-J., Hur, J., 2016. Structural and compositional changes of dissolved organic matter upon solid-phase extraction tracked by multiple analytical tools. Anal. Bioanal. Chem. 408 (23), 6249–6258.

Chen, M., Li, C., Zeng, C., Zhang, F., Raymond, P.A., Hur, J., 2019. Immobilization of relic anthropogenic dissolved organic matter from alpine rivers in the Himalayan-Tibetan Plateau in winter. Water Res. 160, 97–106.

Chen, M., Zeng, C., Zhang, F., Kang, S., Li, C., 2020. Characteristics of dissolved organic matter from a transboundary Himalayan watershed: relationships with land use, elevation, and hydrology. ACS Earth and Space Chemistry 4 (3), 449–456.

Cui, X., Graf, H.-F., 2009. Recent land cover changes on the Tibetan Plateau: a review. Clim. Chang. 94 (1), 47–61.

Fasching, C., Ulseth, A.J., Schelker, J., Steniczka, G., Battin, T.J., 2016. Hydrology controls dissolved organic matter export and composition in an alpine stream and its hyporheic zone. Limnol. Oceanogr. 61 (2), 558–571.
Feng, L., Xu, J.Z., Kang, S.C., Li, X.F., Li, Y., Jiang, B., Shi, Q., 2016. Chemical composition of microbe-derived dissolved organic matter in cryoconite in Tibetan Plateau glaciers: insights from Fourier transform ion cyclotron resonance mass spectrometry analysis. Environmental Science & Technology 50 (24), 13215–13223.
Gao, T.G., Kang, S.C., Chen, R.S., Zhang, T.G., Zhang, T.J., Han, C.T., Tripathee, L., Sillanpaa, M., Zhang, Y.L., 2019. Riverine dissolved organic carbon and its optical properties in a permafrost region of the Upper Heihe River basin in the Northern Tibetan Plateau. Sci. Total Environ. 686, 370–381.
Helms, J.R., Stubbins, A., Ritchie, J.D., Minor, E.C., Kieber, D.J., Mopper, K., 2008. Absorption spectral slopes and slope ratios as indicators of molecular weight, source, and photobleaching of chromophoric dissolved organic matter. Limnol. Oceanogr 53 (3), 955–969.
Holmes, R.M., McClelland, J.W., Peterson, B.J., Tank, S.E., Bulygina, E., Eglinton, T.I., Gordeev, V.V., Gurtovaya, T.Y., Raymond, P.A., Repeta, D.J., Staples, R., Striegl, R.G., Zhulidov, A.V., Zimov, S.A., 2012. Seasonal and annual fluxes of nutrients and organic matter from large rivers to the Arctic Ocean and surrounding seas. Estuar. Coasts 35 (2), 369–382.
Hood, E.W., Williams, M.W., Caine, N., 2002. Yields of dissolved organic C, N, and P. from three high-elevation catchments, Colorado Front Range, U.S.A. Water Air & Soil Pollution Focus 2 (2), 165–180.
Hood, E., Williams, M.W., McKnight, D.M., 2005. Sources of dissolved organic matter (DOM) in a Rocky Mountain stream using chemical fractionation and stable isotopes. Biogeochemistry 74 (2), 231–255.
Hood, E., Fellman, J., Spencer, R.G.M., Hernes, P.J., Edwards, R., D'Amore, D., Scott, D., 2009. Glaciers as a source of ancient and labile organic matter to the marine environment. Nature 462 (7276), 1044–1047.
Hood, E., Battin, T.J., Fellman, J., O'Neel, S., Spencer, R.G.M., 2015. Storage and release of organic carbon from glaciers and ice sheets. Nat. Geosci. 8 (2), 91–96.
Huang, J., Minnis, P., Yi, Y., Tang, Q., Wang, X., Hu, Y., Liu, Z., Ayers, K., Trepte, C., Winker, D., 2007. Summer dust aerosols detected from CALIPSO over the Tibetan Plateau. Geophys. Res. Lett. 34 (18).
Huguet, A., Vacher, L., Relexans, S., Saubusse, S., Froidefond, J.M., Parlanti, E., 2009. Properties of fluorescent dissolved organic matter in the Gironde Estuary. Org. Geochem. 40 (6), 706–719.
Immerzeel, W.W., van Beek, L.P.H., Bierkens, M.F.P., 2010. Climate change will affect the Asian water towers. Science 328 (5984), 1382–1385.
Jaffé, R., Ding, Y., Niggemann, J., Vahatalo, A.V., Stubbins, A., Spencer, R.G.M., Campbell, J., Dittmar, T., 2013. Global charcoal mobilization from soils via dissolution and riverine transport to the oceans. Science 340 (6130), 345–347.
Kaiser, N.K., Quinn, J.P., Blakney, G.T., Hendrickson, C.L., Marshall, A.G., 2011. A novel 9.4 Tesla FTICR mass spectrometer with improved sensitivity, mass resolution, and mass range. Journal of the American Society for Mass Spectrometry 22 (8), 1343–1351.
Kang, S., Xu, Y., You, Q., Flügel, W.-A., Pepin, N., Yao, T., 2010. Review of climate and cryospheric change in the Tibetan Plateau. Environ. Res. Lett. 5 (1), 015101.
Kang, L., Huang, J., Chen, S., Wang, X., 2016. Long-term trends of dust events over Tibetan Plateau during 1961–2010. Atmos. Environ. 125, 188–198.
Knicker, H., 2010. "Black nitrogen" – an important fraction in determining the recalcitrance of charcoal. Org. Geochem. 41 (9), 947–950.
Koch, B.P., Dittmar, T., 2006. From mass to structure: an aromaticity index for high-resolution mass data of natural organic matter. Rapid Communication of Mass Spectrometry 20, 926–932.
Koch, B.P., Witt, M., Engbrodt, R., Dittmar, T., Kattner, G., 2005. Molecular formulae of marine and terrigenous dissolved organic matter detected by electrospray ionization Fourier transform ion cyclotron resonance mass spectrometry. Geochim. Cosmochim. Acta 69 (13), 3299–3308.
Lafrenière, M.J., Sharp, M.J., 2004. The concentration and fluorescence of dissolved organic carbon (DOC) in glacial and nonglacial catchments: interpreting hydrological flow routing and DOC sources. Arct. Antarct. Alp. Res. 36 (2), 156–165.
Lau, K.M., Kim, M.K., Kim, K.M., 2006. Asian summer monsoon anomalies induced by aerosol direct forcing: the role of the Tibetan Plateau. Clim. Dyn. 26, 855.
Leefmann, T., Frickenhaus, S., Koch, B.P., 2019. UltraMassExplorer: a browser-based application for the evaluation of high-resolution mass spectrometric data. Rapid Commun. Mass Spectrom. 33 (2), 193–202.
Li, C., Carme, B., Kang, S., August, A., Chen, P., Zhang, Q., Cong, Z., Chen, B., Qin, D., Örjan, G., 2016a. Sources of black carbon to the Himalayan–Tibetan Plateau glaciers. Nat. Commun. 7, 12574.
Li, C., Chen, P., Kang, S., Yan, F., Li, X., Qu, B., Sillanpää, M., 2016b. Carbonaceous matter deposition in the high glacial regions of the Tibetan Plateau. Atmos. Environ. 141, 203–208.
Li, C., Yan, F., Kang, S., Chen, P., Hu, Z., Han, X., Zhang, G., Gao, S., Qu, B., Sillanpää, M., 2017. Deposition and light absorption characteristics of precipitation dissolved organic carbon (DOC) at three remote stations in the Himalayas and Tibetan Plateau, China. Science of the Total Environment 605-606 (Supplement C), 1039-1046.
Liu, X., Zheng, H., Zhang, M., Liu, C., 2011. Identification of dominant climate factor for pan evaporation trend in the Tibetan Plateau. J. Geogr. Sci. 21 (4), 594–608.
Liu, Y.M., Xu, J.Z., Kang, S.C., Li, X.F., Li, Y., 2016. Storage of dissolved organic carbon in Chinese glaciers. J. Glaciol. 62 (232), 402–406.
Liu, F., Kou, D., Abbott, B.W., Mao, C., Chen, Y., Chen, L., Yang, Y., 2019. Disentangling the effects of climate, vegetation, soil and related substrate properties on the biodegradability of permafrost-derived dissolved organic carbon. Journal of Geophysical Research: Biogeosciences 124 (11), 3377–3389.
Luo, C., Rodriguez-R, L.M., Johnston, E.R., Wu, L., Cheng, L., Xue, K., Tu, Q., Deng, Y., He, Z., Shi, J.Z., Yuan, M.M., Sherry, R.A., Li, D., Luo, Y., Schuur, E.A.G., Chain, P., Tiedje, J.M., Zhou, J., Konstantinidis, K.T., 2014. Soil microbial community responses to a decade of warming as revealed by comparative metagenomics. Appl. Environ. Microbiol. 80 (5), 1777–1786.
Ma, X., Liu, G., Wu, X., Smoak, J.M., Ye, L., Xu, H., Zhao, L., Ding, Y., 2018. Influence of land cover on riverine dissolved organic carbon concentrations and export in the Three Rivers Headwater Region of the Qinghai-Tibetan Plateau. Sci. Total Environ. 630, 314–322.
Malard, F., Tockner, K., Ward, J., 1999. Shifting dominance of subcatchment water sources and flow paths in a glacial floodplain,Val Roseg, Switzerland. Arct. Antarct. Alp. Res. 31, 135.
Malard, F., Uehlinger, U., Zah, R., Tockner, K., 2006. Flood-pulse and riverscape dynamics in a braided glacial river. Ecology 87 (3), 704–716.
Mcknight, D.M., Harnish, R., Wershaw, R.L., Baron, J.S., Schiff, S., 1997. Chemical characteristics of particulate, colloidal, and dissolved organic material in Loch Vale Watershed, Rocky Mountain National Park. Biogeochemistry 36 (1), 99–124.
McKnight, D.M., Boyer, E.W., Westerhoff, P.K., Doran, P.T., Kulbe, T., Andersen, D.T., 2001. Spectrofluorometric characterization of dissolved organic matter for indication of precursor organic material and aromaticity. Limnol. Oceanogr. 46 (1), 38–48.
Messerli, B., Viviroli, D., Weingartner, R., 2004. Mountains of the world: vulnerable water towers for the 21st century. Ambio Special Rep 13, 29–34.
Miehe, G., Schleuss, P.-M., Seeber, E., Babel, W., Biermann, T., Braendle, M., Chen, F., Coners, H., Foken, T., Gerken, T., Graf, H.-F., Guggenberger, G., Hafner, S., Holzapfel, M., Ingrisch, J., Kuzyakov, Y., Lai, Z., Lehnert, L., Leuschner, C., Li, X., Liu, J., Liu, S., Ma, Y., Miehe, S., Mosbrugger, V., Noltie, H.J., Schmidt, J., Spielvogel, S., Unteregelsbacher, S., Wang, Y., Willinghöfer, S., Xu, X., Yang, Y., Zhang, S., Opgenoorth, L., Wesche, K., 2019. The Kobresia pygmaea ecosystem of the Tibetan highlands – origin, functioning and degradation of the world's largest pastoral alpine ecosystem: Kobresia pastures of Tibet. Sci. Total Environ. 648, 754–771.
Mukherji, A., Molden, D., Nepal, S., Rasul, G., Wagnon, P., 2015. Himalayan waters at the crossroads: issues and challenges. International Journal of Water Resources Development 31 (2), 151–160.
Newton, A., 2007. Tibetan dust bowl. Nat. Geosci. https://doi.org/10.1038/ngeo.2007.20.
Osburn, C.L., Anderson, N.J., Stedmon, C.A., Giles, M.E., Whiteford, E.J., McGenity, T.J., Dumbrell, A.J., Underwood, G.J.C., 2017. Shifts in the source and composition of dissolved organic matter in Southwest Greenland Lakes along a regional hydroclimatic gradient. Journal of Geophysical Research: Biogeosciences 122 (12), 3431–3445.
Petrone, K.C., Jones, J.B., Hinzman, L.D., Boone, R.D., 2006. Seasonal export of carbon, nitrogen, and major solutes from Alaskan catchments with discontinuous permafrost. Journal of Geophysical Research: Biogeosciences 111 (G2).
Qiu, J., 2008. The third pole. Nature 454, 393–396.
Qiu, J., 2010. Measuring the meltdown. Nature 468, 141–142.
Qu, B., Aho, K.S., Li, C., Kang, S., Sillanpaa, M., Yan, F., Raymond, P.A., 2017. Greenhouse gases emissions in rivers of the Tibetan Plateau. Sci. Rep. 7 (1), 16573.
Qu, B., Zhang, Y., Kang, S., Sillanpää, M., 2019. Water quality in the Tibetan Plateau: major ions and trace elements in rivers of the "Water Tower of Asia". Sci. Total Environ. 649, 571–581.
Savory, J.J., Kaiser, N.K., McKenna, A.M., Xian, F., Blakney, G.T., Rodgers, R.P., Hendrickson, C.L., Marshall, A.G., 2011. Parts-per-billion Fourier transform ion cyclotron resonance mass measurement accuracy with a "walking" calibration equation. Anal. Chem. 83 (5), 1732–1736.
Shatilla, N.J., Carey, S.K., 2019. Assessing inter-annual and seasonal patterns of DOC and DOM quality across a complex alpine watershed underlain by discontinuous permafrost in Yukon, Canada. Hydrol. Earth Syst. Sci. 23 (9), 3571–3591.
Spencer, R.G.M., Guo, W.D., Raymond, P.A., Dittmar, T., Hood, E., Fellman, J., Stubbins, A., 2014. Source and biolability of ancient dissolved organic matter in glacier and lake ecosystems on the Tibetan Plateau. Geochim. Cosmochim. Acta 142, 64–74.
Stubbins, A., Hood, E., Raymond, P.A., Aiken, G.R., Sleighter, R.L., Hernes, P.J., Butman, D., Hatcher, P.G., Striegl, R.G., Schuster, P., Abdulla, H.A.N., Vermilyea, A.W., Scott, D.T., Spencer, R.G.M., 2012. Anthropogenic aerosols as a source of ancient dissolved organic matter in glaciers. Nat. Geosci. 5 (3), 198–201.
Su, F., Zhang, L., Ou, T., Chen, D., Yao, T., Tong, K., Qi, Y., 2016. Hydrological response to future climate changes for the major upstream river basins in the Tibetan Plateau. Global and Planetary Change 136 (Supplement C), 82–95.
Thapa, P., Xu, J.Z., Neupane, B., Rupakheti, D., 2020. Chemical composition of inorganic and organic species in snow/ice in the glaciers of western China. Sci. Total Environ. 706.
Thompson, L.G., Yao, T., Mosley-Thompson, E., Davis, M.E., Henderson, K.A., Lin, P.-N., 2000. A high-resolution millennial record of the South Asian Monsoon from Himalayan ice cores. Science 289 (5486), 1916–1919.
Tong, K., Su, F., Yang, D., Zhang, L., Hao, Z., 2014. Tibetan Plateau precipitation as depicted by gauge observations, reanalyses and satellite retrievals. Int. J. Climatol. 34 (2), 265–285.
Wang, Z.-w., Wang, Q., Zhao, L., Wu, X.-d., Yue, G.-y., Zou, D.-f., Nan, Z.-t., Liu, G.-y., Pang, Q.-q., Fang, H.-b., Wu, T.-H., Shi, J.-z., Jiao, K.-q., Zhao, Y.-h., Zhang, L.-l., 2016. Mapping the vegetation distribution of the permafrost zone on the Qinghai-Tibet plateau. J. Mt. Sci. 13 (6), 1035–1046.
Wang, X., Zheng, D., Shen, Y., 2008. Land use change and its driving forces on the Tibetan Plateau during 1990–2000. Catena 72 (1), 56–66.
Wang, Y., Spencer, R.G.M., Podgorski, D.C., Kellerman, A.M., Rashid, H., Zito, P., Xiao, W., Wei, D., Yang, Y., Xu, Y., 2018. Spatiotemporal transformation of dissolved organic matter along an alpine stream flow path on the Qinghai–Tibet Plateau: importance of source and permafrost degradation. Biogeosciences 15 (21), 6637–6648.
Wang, C., Gao, Q., Yu, M., 2019. Quantifying trends of land change in Qinghai-Tibet Plateau during 2001–2015. Remote Sens. 11, 2435.

Weishaar, J.L., Aiken, G.R., Bergamaschi, B.A., Fram, M.S., Fujii, R., Mopper, K., 2003. Evaluation of Specific Ultraviolet Absorbance as an Indicator of the Chemical Composition and Reactivity of Dissolved Organic Carbon. Environ. Sci. Technol. 37 (20), 4702–4708.

Wilson, H.F., Raymond, P.A., Saiers, J.E., Sobczak, W.V., Xu, N., 2016. Increases in humic and bioavailable dissolved organic matter in a forested New England headwater stream with increasing discharge. Mar. Freshw. Res. 67 (9), 1279–1292.

Wu, L.L., Huh, Y.S., 2007. Dissolved reactive phosphorus in large rivers of East Asia. Biogeochemistry 85 (3), 263–288.

Xian, F., Hendrickson, C.L., Blakney, G.T., Beu, S.C., Marshall, A.G., 2010. Automated broadband phase correction of Fourier transform ion cyclotron resonance mass spectra. Anal. Chem. 82 (21), 8807–8812.

Xu, Z.X., Gong, T.L., Li, J.Y., 2008. Decadal trend of climate in the Tibetan Plateau—regional temperature and precipitation. Hydrol. Process. 22 (16), 3056–3065.

Xu, B., Cao, J., Hansen, J., Yao, T., Joswia, D.R., Wang, N., Wu, G., Wang, M., Zhao, H., Yang, W., Liu, X., He, J., 2009. Black soot and the survival of Tibetan glaciers. Proc. Natl. Acad. Sci. 106 (52), 22114–22118.

Yan, F., Kang, S., Li, C., Zhang, Y., Qin, X., Li, Y., Zhang, X., Hu, Z., Chen, P., Li, X., Qu, B., Sillanpaa, M., 2016. Concentration, sources and light absorption characteristics of dissolved organic carbon on a medium-sized valley glacier, northern Tibetan Plateau. Cryosphere 10 (6), 2611–2621.

Yang, M., Nelson, F.E., Shiklomanov, N.I., Guo, D., Wan, G., 2010. Permafrost degradation and its environmental effects on the Tibetan Plateau: a review of recent research. Earth Sci. Rev. 103 (1), 31–44.

Yao, T., Pu, J., Lu, A., Wang, Y., Yu, W., 2007. Recent glacial retreat and its impact on hydrological processes on the Tibetan Plateau, China, and surrounding regions. Arct. Antarct. Alp. Res. 39 (4), 642–650.

Yin, A., Harrison, T.M., 2000. Geologic evolution of the Himalayan-Tibetan orogen. Annu. Rev. Earth Planet. Sci. 28 (1), 211–280.

Zeng, Y., Feng, Z., Cao, G., 2003. Land cover change and its environmental impact in the upper reaches of the Yellow River, Northeast Qinghai-Tibetan Plateau. Mt. Res. Dev. 23 (4), 353–361 (9).

Zhang, J., Wang, J.T., Chen, W., Li, B., Zhao, K., 1988. Vegetation of Xizang (Tibet). Science Press, Beijing.

Zhang, X.Y., Arimoto, R., An, Z.S., 1997. Dust emission from Chinese desert sources linked to variations in atmospheric circulation. Journal of Geophysical Research: Atmospheres 102 (D23), 28041–28047.

Zhang, T., Heginbottom, J.A., Barry, R.G., Brown, J., 2000. Further statistics on the distribution of permafrost and ground ice in the Northern Hemisphere. Polar Geogr. 24 (2), 126–131.

Zhang, T., Barry, R.G., Knowles, K., Heginbottom, J.A., Brown, J., 2008. Statistics and characteristics of permafrost and ground-ice distribution in the Northern Hemisphere. Polar Geogr. 31 (1–2), 47–68.

Zhao, Z., Liu, G., Mou, N., Xie, Y., Xu, Z., Li, Y., 2018a. Assessment of carbon storage and its influencing factors in Qinghai-Tibet plateau. Sustainability 10 (6), 1864.

Zhao, L., Wu, X., Wang, Z., Sheng, Y., Fang, H., Zhao, Y., Hu, G., Li, W., Pang, Q., Shi, J., Mo, B., Wang, Q., Ruan, X., Li, X., Ding, Y., 2018b. Soil organic carbon and total nitrogen pools in permafrost zones of the Qinghai-Tibetan Plateau. Sci. Rep. 8 (1), 3656.

Zou, D., Zhao, L., Sheng, Y., Chen, J., Hu, G., Wu, T., Wu, J., Xie, C., Wu, X., Pang, Q., Wang, W., Du, E., Li, W., Liu, G., Li, J., Qin, Y., Qiao, Y., Wang, Z., Shi, J., Cheng, G., 2017. A new map of permafrost distribution on the Tibetan Plateau. Cryosphere 11 (6), 2527–2542.

Zsolnay, A., Baigar, E., Jimenez, M., Steinweg, B., Saccomandi, F., 1999. Differentiating with fluorescence spectroscopy the sources of dissolved organic matter in soils subjected to drying. Chemosphere 38 (1), 45–50.